The Measurement of Backscatter Coefficient from a Broadband Pulse-Echo System: A New Formulation

Xucai Chen, Dan Phillips, Karl Q. Schwarz, Jack G. Mottley, and Kevin J. Parker, *Fellow, IEEE*

***Abstract*—A new formulation for obtaining the absolute backscatter coefficient from pulse-echo measurements is presented. Using this formulation, performing the diffraction correction and system calibration is straightforward. The diffraction correction function for the measurement of backscatter coefficient and the acoustic coupling function for a pulse-echo system are defined. Details of these functions for two very useful cases are presented: a flat disk transducer and a spherically focused transducer. Approximations of these functions are also provided. For a flat disk transducer, the final formulation appears as a modification to the established Sigelmann-Reid formulation. For a focused transducer, the final correction is a weak function of frequency when the scattering volume is near the focal area, rather than the frequency squared dependence proposed by earlier investigators.**

I. Introduction

In tissue characterization , the "backscatter coefficient" is a parameter that describes the effectiveness with which the tissue scatters ultrasound energy. Recovering this parameter from a pulse-echo system has been pursued by many investigators. The American Institute of Ultrasound in Medicine (AIUM) [1] recommends that "measurements of the backscatter coefficient in phantom materials should be made using the Sigelmann-Reid [2] technique", where the farfield of a flat transducer is used, and system calibration is accomplished by substitution with a reference plate. In the final data reduction, the area of the transducer beam appears as a correction factor. This has caused some confusion, since some investigators used the -3 dB beamwidth while others used the -6 dB beamwidth. Alternative techniques and methods of data reduction have been proposed [3]–[5]. System normalization is replaced by a volume integral of the pressure distribution pattern and the distribution function of the scatterers in the method of Campbell and Waag. [3] A similar integral is developed in the method given by Madsen *et al.* [4]

We have developed another formulation for the data reduction of the absolute backscatter coefficient from pulse-echo measurements. This formulation uses simple functions with tractable approximations which are, in some instances, simple constants. In Section II, the sonar equations for a single scatterer as well as a distribution of scatterers are derived. The diffraction correction function is defined. The effect of the attenuation is included by using complex wave numbers and is elaborated in Appendix B. System calibration is discussed, and the acoustic coupling correction coefficient is defined. In Section III, the diffraction correction function and the acoustic coupling function for two very useful cases are presented: the flat disk transducer and the spherically focused transducer. Approximations of these functions are provided. In Section IV, the new formulation is compared with established methods. The AIUM recommended Sigelmann-Reid method is derived as a special case of our formulation for a flat transducer, and a modification to their formulation is proposed. The formulation for the focused transducer given by Madsen *et al.* [4] is also evaluated. For simplicity, the pulse duration is assumed to be much smaller than the receiver time gate duration. The modification to the backscatter formulation due to this simplification is discussed in Appendix A. The effect of coherent scattering can be ignored under this assumption. [4]

Manuscript received December 20, 1995; accepted July 31, 1996. This work was supported in part by the National Institutes of Health, grant no. CA 44732, and National Science Foundation grant EEC9209615.

The authors are with the Rochester Center for Biomedical Ultrasound, University of Rochester, Rochester, NY 14627 (e-mail: xucaichen@echocardio.medicine.rochester.edu).

II. The Basic Formulation

A. The Incident Wave

In the following discussion, a broadband pulse-echo system is assumed. Frequency domain analysis will be used, where the time and frequency domain representations of any signal are related by the Fourier transform pair:

$$\begin{cases} p(t) = \dfrac{1}{2\pi}\displaystyle\int_{-\infty}^{\infty} P(\omega)\exp(-i\omega t)d\omega, \\ P(\omega) = \displaystyle\int_{-\infty}^{\infty} p(t)\exp(i\omega t)dt, \end{cases} \tag{1}$$

and $\omega = 2\pi f$ is the angular frequency of the acoustic wave. Since $p(t)$ is real, we have $P(-\omega) = P^*(\omega)$. The geometry of a typical measurement system is shown in Fig. 1, where the material or tissue to be measured is surrounded by a well-characterized fluid medium. The surrounding medium has density ρ_0 and sound speed c_0. In general, c_0 is complex, so that the wave number $k = \omega/c_0$ is also complex. In the transmission mode, the transducer surface is driven

into oscillation by an electrical excitation such that the normal velocity distribution on the transducer surface is $U_T(\mathbf{r}_T;\omega)$. The incident pressure field at $\mathbf{r}$, denoted by $P_{in}(\mathbf{r};\omega)$ in the frequency domain, can be written as

$$P_{in}(\mathbf{r};\omega) = P_0(\omega)D_T(\mathbf{r};\omega); \tag{2}$$

where $P_0(\omega) = \rho_0 c_0 U(\omega)$ is the characteristic pressure amplitude at the transducer surface, $U(\omega)$ is the overall normal velocity on the transducer surface, and $D_T(\mathbf{r};\omega)$ is the radiation pattern defined as

$$D_T(\mathbf{r};\omega) = \frac{-ik}{2\pi}\iint_{S_T}\frac{U_T(\mathbf{r}_T;\omega)}{U(\omega)}\frac{\exp(ikr'_T)}{r'_T}dS(\mathbf{r}_T), \tag{3}$$

where $U_T(\mathbf{r}_T;\omega)/U(\omega)$ can be regarded as the relative sensitivity and phase delay of each transducer element, and $r'_T = |\mathbf{r}-\mathbf{r}_T|$ is the distance from the point source on the transducer surface to the point of observation. Using this definition of the radiation pattern, the transducer can be focused either geometrically or dynamically through phase delays. This expression for the radiation pattern is rigorous for a transducer with active element larger than the acoustic wavelength ($ka \gg 1$).

B. The Received Scattered Wave from a Single Scatterer

For a single scatterer located at $\mathbf{r}$, the scattered pressure $P_s(\mathbf{r},\mathbf{r}_s;\omega)$ far away from the scatterer ($kr_s \gg 1$) can be written as

$$P_s(\mathbf{r},\mathbf{r}_s;\omega) = P_{in}(\mathbf{r};\omega)\Phi_s(\mathbf{r};\omega)\exp(ikr_s)/r_s, \tag{4}$$

where $\Phi_s(\mathbf{r};\omega)$ is the scattering amplitude function, and $\mathbf{r}_s$ is measured from the scatterer to the observation point. The scattering amplitude depends on the size and shape of the scatterer, as well as its compressibility contrast, $\gamma_\kappa = (\kappa-\kappa_0)/\kappa_0$, and density contrast, $\gamma_\rho = (\rho-\rho_0)/\rho$, relative to the surrounding medium, and the scattering angle, $\theta_s = \arccos(\mathbf{k}_{in}\cdot\mathbf{k}_s/k^2)$. When the scatterer is small compared with the wavelength, the Rayleigh approximation can be used, *i.e.*

$$\Phi_s = \frac{k^2 a_s^3}{3}\left(\gamma_\kappa + \frac{\gamma_\rho}{1-\gamma_\rho/3}\cos\theta_s\right). \tag{5}$$

For a weak scatterer with $|\gamma_\rho| \ll 1$, we have the Born approximation

$$\Phi_s = \frac{k^2 a_s^3}{3}(\gamma_\kappa + \gamma_\rho\cos\theta_s). \tag{6}$$

Using this definition, the differential scattering cross-section of the scatterer is given by $\sigma_d(\mathbf{r};\omega) = |\Phi_s(\mathbf{r};\omega)|^2$. Since the scattering angle at the surface of the transducer is nearly 180° for $r_s \gg a$, it will be treated as a constant in the following discussion.

The scattered acoustic pressure received by a phase sensitive transducer due to the presence of the single scatterer can be expressed as the average of $P_s(\mathbf{r};\omega)$ on the transducer surface, *i.e.*

$$\overline{P}_s(\mathbf{r};\omega) = \frac{1}{S_R}\int_{S_R}\frac{U_R(\mathbf{r};\omega)}{U(\omega)}P_s(\mathbf{r},\mathbf{r}_s;\omega)dS(\mathbf{r}_R), \tag{7}$$

where S_R is the area of the active transducer element, and $U_R(\mathbf{r};\omega)/U(\omega)$ can be regarded as the relative sensitivity and phase delay of a receiver element. Let us define

$$D_R(\mathbf{r};\omega) = \frac{-ik}{2\pi}\iint_{S_R}\frac{U_R(\mathbf{r}_R;\omega)}{U(\omega)}\frac{\exp(ikr'_R)}{r'_R}dS_R(\mathbf{r}_R), \tag{8}$$

as the radiation pattern of the receiver, where $r'_R = r_s$ is the distance from the point receiver on the transducer surface to the point of observation. Combining (6-8), we have

$$\overline{P}_s(\mathbf{r};\omega) = P_0(\omega)D_T(\mathbf{r};\omega)[i2\pi\Phi_s(\mathbf{r};\omega)/(k\cdot S_R)]D_R(\mathbf{r};\omega). \tag{9}$$

Eq. (9) is analogous to the sonar equation for a single scatterer where $i2\pi\Phi_s(\mathbf{r};\omega)/(k\cdot S_R)$ is the target response. In time domain, $\overline{p}_s(\mathbf{r};t)$ is localized around $t = 2r/c$ under most pulse-echo conditions.

Since the transmitter and the receiver are identical and reversible transducers, we have

$$D_T(\mathbf{r};\omega) = D_R(\mathbf{r};\omega) \equiv D(\mathbf{r};\omega). \tag{10}$$

In the following discussion, we will continue to use different transmitter and receiver radiation pattern nomenclature, when necessary, to help keep track of the derivation.

C. The Received Scattered Wave from an Inhomogeneity

The scattered pressure wave from an inhomogeneity can be expressed as [6]

$$P_s(\mathbf{r},\mathbf{r}_s;\omega) = \iiint_V \left[k^2\gamma_\kappa(\mathbf{r})P(\mathbf{r};\omega)g(\mathbf{r}_s|\mathbf{r};\omega) + \gamma_\rho(\mathbf{r})\nabla P(\mathbf{r};\omega)\bullet\nabla g(\mathbf{r}_s|\mathbf{r};\omega)\right]dV(\mathbf{r}) \tag{11}$$

where $P(\mathbf{r};\omega)$ is the pressure in the medium, $g(\mathbf{r}_s|\mathbf{r};\omega) = \exp(ikr_s)/4\pi r_s$ is the three-dimensional free-space Green's function, and the gradient operator is with respect to $\mathbf{r}$. When the observation point is far away from the scattering region ($kr_s \gg 1$), we have

$$\nabla g(\mathbf{r}_s|\mathbf{r};\omega) \approx \frac{\exp(ikr_s)}{4\pi r_s}(-i\mathbf{k}_s). \tag{12}$$

Now let us assume that over the volume of interest the pressure distribution is not far different from a plane wave such that $\nabla P(\mathbf{r};\omega) = P(\mathbf{r};\omega)(i\mathbf{k}_{in})$, or

$$\nabla D_T(\mathbf{r};\omega) \approx D_T(\mathbf{r};\omega)(i\mathbf{k}_{in}), \tag{13}$$

then (11) can be written as

$$P_s(\mathbf{r},\mathbf{r}_s;\omega) = P_0(\omega)\iiint_V \frac{k^2\exp(ikr_s)}{4\pi r_s}\gamma_{\kappa\rho}(\mathbf{r})D_T(\mathbf{r};\omega)dV(\mathbf{r}) \tag{14}$$

where $\gamma_{\kappa\rho}(\mathbf{r}) = \gamma_\kappa(\mathbf{r}) + \gamma_\rho(\mathbf{r})\cos\theta_s$ is the combined compressibility and density contrast at $\mathbf{r}$, and $\cos\theta_s = \mathbf{k}_{in} \cdot \mathbf{k}_s/k^2$.

The scattered pressure, detected by the receiver, is the average over the receiver surface, as defined by (7). Then

$$\overline{P}_s(\mathbf{r} \in V;\omega) = P_0(\omega)\frac{ik}{2S_R} \cdot \iiint_V D_T(\mathbf{r};\omega)\gamma_{\kappa\rho}(\mathbf{r})D_R(\mathbf{r};\omega)dV(\mathbf{r}) \tag{15}$$

where $D_T(\mathbf{r};\omega)$ is the radiation pattern of the transmitter, and $D_R(\mathbf{r};\omega)$ is the radiation pattern of the receiver, as defined earlier. Since $D_T(\mathbf{r};\omega) = D_R(\mathbf{r};\omega)$ from (10), $D(\mathbf{r};\omega)$ will be used in later discussions.

The scattered power as received by the phase sensitive transducer is therefore (except for a constant for unit conversion)

$$|\overline{P}_s(\mathbf{r} \in V;\omega)|^2 = |P_0(\omega)|^2\left(\frac{k}{2S_R}\right)^2 \cdot \iiint_V \iiint_V D^2(\mathbf{r};\omega)D^{*2}(\mathbf{r}';\omega) \times \gamma_{\kappa\rho}(\mathbf{r})\gamma^*_{\kappa\rho}(\mathbf{r}')dV(\mathbf{r})dV(\mathbf{r}'). \tag{16}$$

The mean power is calculated from

$$\left\langle|\overline{P}_s(\mathbf{r} \in V;\omega)|^2\right\rangle = |P_0(\omega)|^2\left(\frac{k}{2S_R}\right)^2 \cdot \iiint_V \iiint_V D^2(\mathbf{r};\omega)D^{*2}(\mathbf{r}';\omega) \times \left\langle\gamma_{\kappa\rho}(\mathbf{r})\gamma^*_{\kappa\rho}(\mathbf{r}')\right\rangle dV(\mathbf{r})dV(\mathbf{r}'), \tag{17}$$

where $\left\langle\gamma_{\kappa\rho}(\mathbf{r})\gamma^*_{\kappa\rho}(\mathbf{r}')\right\rangle$ is the auto-correlation function of $\gamma_{\kappa\rho}(\mathbf{r})$ and is dependent on the distance $|\mathbf{r}_\Delta|$ only, where $\mathbf{r}_\Delta = \mathbf{r}' - \mathbf{r}$. From (13), we have $D(\mathbf{r}';\omega) \approx D(\mathbf{r};\omega)\exp(i\mathbf{k}_{in}\cdot\mathbf{r}_\Delta)$ for $\mathbf{k}_{in}\cdot\mathbf{r}_\Delta \ll 1$. If $|D(\mathbf{r};\omega)|^4$ does not change significantly over the correlation length of $\gamma_{\kappa\rho}(\mathbf{r})$, the integrals in the above equation can be de-coupled. Then (17) becomes

$$\left\langle|\overline{P}_s(\mathbf{r} \in V;\omega)|^2\right\rangle = |P_0(\omega)|^2\eta(\omega) \times \left[\left(\frac{2\pi}{kS_R}\right)^2 \iiint_V |D(\mathbf{r};\omega)|^4 dV(\mathbf{r})\right], \tag{18}$$

where integration is over the whole volume the scatterers occupy, and $\eta(\omega)$ is defined as

$$\eta(\omega) = \left(\frac{k^2}{4\pi}\right)^2 \iiint_V \langle\gamma_{\kappa\rho}(\mathbf{r})\gamma_{\kappa\rho}(\mathbf{r}+\mathbf{r}_\Delta)\rangle \times \exp(-i2\mathbf{k}_{in}\cdot\mathbf{r}_\Delta)dV(\mathbf{r}_\Delta). \tag{19}$$

A similar but more detailed analysis of the double volume integral is provided by Campbell and Waag [3].

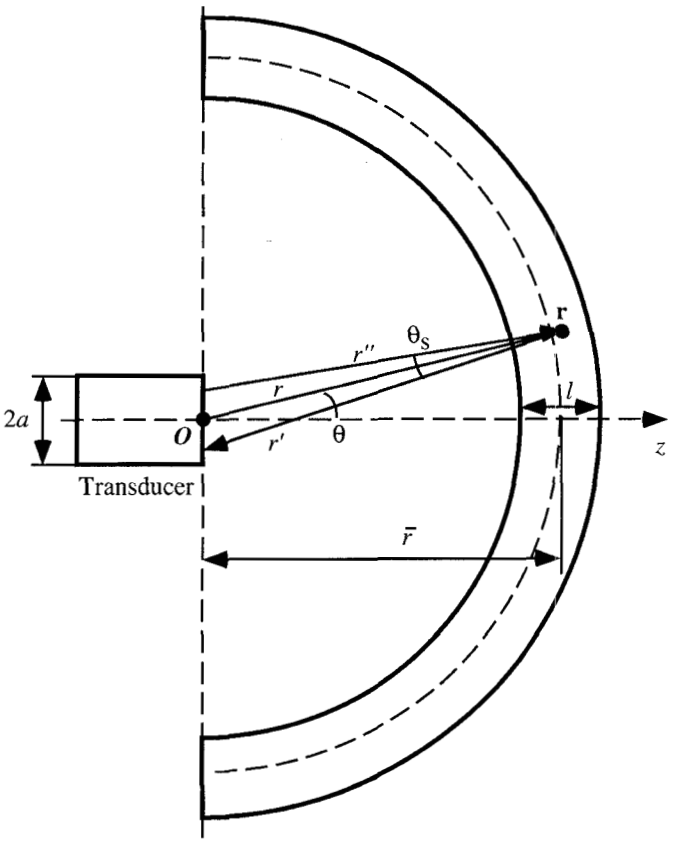

Fig. 1. Scattering geometry.

Experimentally, scatterers are often present outside the volume of interest, and a receiver time-gate $t = [t_1, t_2]$ is used to select a sample volume. Thus the integration is over a finite volume bounded by the two hemispherical surfaces as depicted in Fig. 1. Let us define the mean diffraction correction function for the backscatter measurement as

$$\overline{D}_s(\mathbf{r} \in V;\omega) = \frac{1}{l}\left[\left(\frac{2\pi}{kS_R}\right)^2 \iiint_V |D(\mathbf{r};\omega)|^4 dV(\mathbf{r})\right] \tag{20}$$

where $l = c\tau/2$ is the length of the sample, and $\tau = t_2 - t_1$ is the duration of the receiver gate. Then (18) takes the form of

$$\left\langle|\overline{P}_s(\mathbf{r} \in V;\omega)|^2\right\rangle = |P_0(\omega)|^2\eta(\omega)\cdot l\cdot\overline{D}_s(\mathbf{r} \in V;\omega). \tag{21}$$

D. An Ensemble of Discrete Scatterers

When a distribution of discrete scatterers are present in the acoustic field, the received echo is the sum of individual echoes, *i.e.*

$$\overline{P}_s(\mathbf{r}_j;\omega) = \sum_{j=1}^{N}\overline{P}_s(\mathbf{r}_j;\omega) = P_0(\omega)\sum_{j=1}^{N}D^2(\mathbf{r}_j;\omega)\cdot[i2\pi\Phi_s(\mathbf{r};\omega)/(k\cdot S_R)], \tag{22}$$

where $\Phi_s(\mathbf{r};\omega) = \frac{k^2 a_s^3}{3}(\gamma_\kappa - \gamma_\rho)$ is the backscatter amplitude function of an individual scatterer. For simplicity, the scatterers are assumed to be identical spheres. When the scatterers are randomly distributed, the scattered power from the scattering region can be derived using the same procedure discussed for scattering from an inhomogeneity. For discrete scatterers, we have

$$\gamma_{\kappa\rho}(\mathbf{r}) = \begin{cases} \gamma_\kappa - \gamma_\rho, & \text{inside a scatterer,} \\ 0, & \text{otherwise} \end{cases} \tag{23}$$

Let n_0 be the number density of the scatterers, then for an elementary volume dV there are $n_0 dV$ scatterers. The auto-correlation function of $\gamma_{\kappa\rho}(\mathbf{r})$ can be found from geometrical considerations as

$$\langle \gamma_{\kappa\rho}(\mathbf{r})\gamma_{\kappa\rho}(\mathbf{r}+\mathbf{r}_\Delta)\rangle = \begin{cases} n_0\left(\frac{4\pi a_s^3}{3}\right)(\gamma_\kappa - \gamma_\rho)^2 \\ \quad \times \left(1 - \frac{3|\mathbf{r}_\Delta|}{4a_s} + \frac{|\mathbf{r}_\Delta|^3}{16a_s^3}\right), & 0 \le |\mathbf{r}_\Delta| \le 2a_s, \\ 0. & \text{Otherwise.} \end{cases} \tag{24}$$

The value of the auto-correlation function at $|\mathbf{r}_\Delta| = 0$ is the mean square value of the compressibility-density contrast, which is easily proved since $n_0(4\pi a_s^3/3)$ is the volume fraction of the total discrete scatterers. Substituting into (19), we find the backscatter coefficient of the distribution of scatterers under that condition $ka_s \ll 1$ is

$$\eta(\omega) = n_0 \sigma_d(\omega), \tag{25}$$

where $\sigma_d(\omega) = |\Phi_s(\mathbf{r};\omega)|^2$ is the differential backscatter cross-section of each individual scatterer. Equation (25) indicates that the backscatter coefficient is the mean backscatter cross-section per unit volume.

E. System Calibration

Using electrical equivalent, (21) can be written as

$$\left\langle |V_s(\mathbf{r}\in V;\omega)|^2 \right\rangle = |V_{in}(\omega)\cdot X_T(\omega)\cdot X_R(\omega)|^2 \cdot \eta(\omega) \cdot l \cdot \overline{D}_s(\mathbf{r}\in V;\omega), \tag{26}$$

where $V_s(\mathbf{r}\in V;\omega)$ is the received voltage signal from the scattering volume, $V_{in}(\omega)$ is the electrical signal driving the transducer, $X_T(\omega) = P_0(\omega)/V_{in}(\omega)$ is the electromechanical coupling factor of the transducer in transmit mode, and $X_R(\omega) = V_s(\mathbf{r};\omega)/\overline{P}_s(\mathbf{r};\omega)$ is electromechanical coupling factor of the transducer in receive mode.

In (26), the backscatter coefficient $\eta(\omega)$ is actually the parameter of interest. Since $\overline{D}_s(\mathbf{r}\in V;\omega)$ can be obtained either analytically or numerically, $\eta(\omega)$ can be calculated if the system response function $|V_{in}(\omega)\cdot X_T(\omega)\cdot X_R(\omega)|^2$ is obtained. It is important to stress here that using the formulation given by (26), the system response function does not include the radiation pattern of the transducer. In the Sigelmann and Reid technique, [2] the system response function is measured by putting a perfectly reflecting reference plate at the location of the sample volume. Others have suggested putting the reference plate at half that distance. We will demonstrate later that the most convenient position is in the nearfield for a flat transducer and in the geometrical focal plane for a focused transducer.

It is instructive to note that if a perfectly reflective planar target of large extent is located perpendicular to the acoustic axis z_{ref} away from the transducer surface, the reflected acoustic pressure detected by the transducer is equal to the average acoustic pressure from an identical transducer placed $2z_{\text{ref}}$ away, *i.e.*

$$\overline{P}_{\text{ref}}(z_{\text{ref}};\omega) = \frac{1}{S_R}\int_{S_R} \frac{U_R(\mathbf{r}_R;\omega)}{U(\omega)} P_{\text{in}}(\mathbf{r}|_{z=2z_{\text{ref}}};\omega) dS(\mathbf{r}_R) \tag{27}$$

where $P_{\text{in}}(\mathbf{r};\omega) = P_0(\omega)D_T(\mathbf{r};\omega)$ is the transmitted pressure field at $\mathbf{r}$, $U_R(\mathbf{r}_R;\omega)/U(\omega)$ is the relative sensitivity of the receiver element at $\mathbf{r}_R$, as defined earlier, and the integration is over the surface of the receiver. Define

$$D_{\text{ref}}(2z_{\text{ref}};\omega) = \frac{\exp(-2ikz_{\text{ref}})}{S_R}\int_{S_R} \frac{U_R(\mathbf{r}_R;\omega)}{U(\omega)} \times D_T(2z_{\text{ref}};\omega) dS(\mathbf{r}_R) \tag{28}$$

as the acoustic coupling function from the transducer surface to the reference plane and back to the transducer surface [7], then (27) becomes

$$\overline{P}_{\text{ref}}(z_{\text{ref}};\omega) = P_0(\omega)\cdot \exp(i2kz_{\text{ref}}) D_{\text{ref}}(2Z_{\text{ref}};\omega). \tag{29}$$

Using the same electro-mechanical coupling factors defined earlier, the voltage output due to the reflective wave at the transducer is

$$V_{\text{ref}}(z_{\text{ref}};\omega) = V_{\text{in}}(\omega)X_T(\omega)X_R(\omega)\exp(i2kz_{\text{ref}})D_{\text{ref}}(2z_{\text{ref}};\omega). \tag{30}$$

Combining (26) and (30), we find the backscatter coefficient is

$$\eta(\omega) = \frac{\left\langle |V_s(\mathbf{r}\in V;\omega)|^2 \right\rangle}{|V_{\text{ref}}(2z_{\text{ref}};\omega)|^2} \cdot \frac{|D_{\text{ref}}(2z_{\text{ref}};\omega)|^2}{l\cdot \overline{D}_s(\mathbf{r}\in V;\omega)}, \tag{31}$$

to which the transmission loss through the medium-tissue interface and attenuation correction can be incorporated to arrive at

$$\eta(\omega) = \frac{\left\langle |V_s(\mathbf{r}\in V;\omega)|^2 \right\rangle}{|V_{\text{ref}}(2z_{\text{ref}};\omega)|^2} \cdot \frac{|D_{\text{ref}}(2z_{\text{ref}};\omega)|^2}{\xi^4 \cdot A_s(\bar{r};\omega)\cdot l\cdot \overline{D}_s(\bar{r};\omega)}, \tag{32}$$

where

$$\xi^4 = \left(\frac{2\sqrt{\rho c\cdot \rho_0 c_0}}{\rho c + \rho_0 c_0}\right)^4 = \frac{16(\rho c/\rho_0 c_0)^2}{(1+\rho c/\rho_0 c_0)^4} \tag{33}$$

represents the transmission loss, $\rho_0 c_0$ and ρc being the acoustic impedance of the medium and the tissue, respectively, and $A_s(\bar{r};\omega)$ represents the attenuation correction derived in Appendix B.

III. Specific Applications

From (31) and (32), the backscatter coefficient $\eta(\omega)$ is obtained from two measurements, the power spectra of the backscatter signal and the reflected signal from a flat reference plate. The final data reduction involves the computation of the mean diffraction correction coefficient for backscatter $\overline{D}_s(\mathbf{r} \in V;\omega)$, defined in (20), and the coupling function $D_{\text{ref}}(2z_{\text{ref}};\omega)$, defined in (28). In general, the computation of $\overline{D}_s(\mathbf{r} \in V;\omega)$ involves a surface integral over the surface of the transducer, followed by a volume integral over the space the scatterers occupy; and the computation of $D_{\text{ref}}(2z_{\text{ref}};\omega)$ involves a surface integral over the transducer, followed by another surface integral over the surface of the "mirror" transducer. Fortunately, it is possible to reduce these tedious and complex computations into simple function evaluations for some very important applications.

The mean diffraction correction function for the backscatter measurement, defined in (20), can be regarded as the mean value of $D_s(r;\omega)$ along the length of the sample, *i.e.*

$$\overline{D}_s(\mathbf{r} \in V;\omega) = \frac{1}{l}\int_{\bar{r}-l/2}^{\bar{r}+l/2} D_s(r;\omega)dr, \tag{34}$$

where $\bar{r}$ is the mean distance from the transducer surface to the sample volume, and $D_s(r;\omega)$ is the diffraction correction function defined as

$$D_s(r;\omega) = \left(\frac{2\pi}{kS_R}\right)\iint_r |D(\mathbf{r};\omega)|^4 dS(\mathbf{r}), \tag{35}$$

where the integration is over the hemispherical surface with a radius r, as depicted in Fig. 1.

The integral in (34) can be replaced by $\overline{D}_s(\mathbf{r} \in V;\omega) \cong D_s(\bar{r};\omega)$ if $D_s(r;\omega)$ does not vary significantly over the integral length, as is the case in many practical situations.

Due to the finite length of the transmitted pulse, the integration volume is actually more complicated than given here. A more detailed discussion is included in Appendix A, where a spatial receiving gate is defined. The discussion given here is valid when the pulse duration is much smaller than the receiving gate duration.

A. The Flat Disk Transducer

For a flat disk transducer, the relative sensitivity of the transducer surface can be written as

$$U_T(\mathbf{r}_T;\omega)/U(\omega) = \begin{cases} 1, & |\mathbf{r}_T| \le a, \\ 0, & \text{otherwise}, \end{cases} \tag{36}$$

where a is the radius of the active element. The diffraction pattern of such a transducer has been solved in many forms. Using the spherical coordinates shown in Fig. 1 and the diffraction pattern given in Chen *et al.* [8], we have

$$|D(\mathbf{r};\omega)|^4 = |\exp(ikr)|^4 \left[u_1(Y,Z)^2 + u_2(Y,Z)^2\right]^2 \tag{37}$$

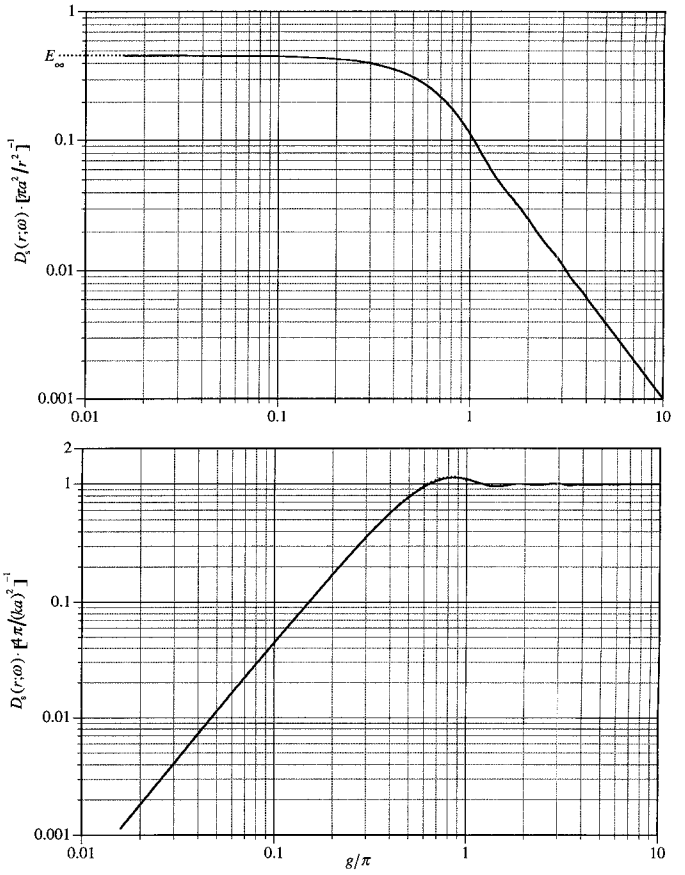

Fig. 2. Diffraction correction coefficient $D_s(r;\omega)$ vs. g/π, normalized by $\pi a^2/r^2$ (top) and $4\pi/(ka)^2$ (bottom). For the flat disk transducer, $g = ka^2/2r$; for the focused transducer, $g = G_p(r_0/r - 1)$. Dashed lines represent the approximations. The approximations are almost indistinguishable from the numerical results for the scales used.

where $Y = ka^2/r$, $Z = ka\sin\theta$, and $u_1(Y,Z)$ and $u_2(Y,Z)$ are the Lommel function of the first order and second order, given by, respectively

$$\begin{cases} u_1(Y,Z) = \displaystyle\sum_{n=0}^{\infty}(-1)^n\left(\frac{Y}{Z}\right)^{2n+1} J_{2n+1}(Z), \\ u_2(Y,Z) = \displaystyle\sum_{n=0}^{\infty}(-1)^n\left(\frac{Y}{Z}\right)^{2n+2} J_{2n+2}(Z). \end{cases} \tag{38}$$

and $J_n(Z)$ is the n-th order cylindrical Bessel function. Substituting into (35), we have

$$D_s(r;\omega) = \frac{\pi a^2}{r^2}\int_{Z=0}^{Z=ka} 8\left\{[u_1(Y,Z)Z/Y]^2 + [u_2(Y,Z)Z/Y]^2\right\}^2 Z^{-3}\left[1-\left(\frac{Z}{ka}\right)^2\right]^{-\frac{1}{2}} dZ. \tag{39}$$

This integral is readily evaluated using the method discussed in Chen *et al.* [8] where alternative formulations of (38) are provided for specific values of Y and Z.

Fig. 2 shows $D_s(r;\omega)$ plotted against $g \equiv Y/2 = ka^2/2r$ on logarithmic scale, normalized by $\pi a^2/r^2$. The parameter g can be considered as a normalized distance from the

transducer to the scatterer location. The dependence of $D_s(r;\omega)$ on g can be divided into two intervals, $g < \pi$ and $g > \pi$. For $g < \pi$, the variation of $D_s(r;\omega)$ is relatively slow, while for $g > \pi$, $D_s(r;\omega)$ is nearly inversely proportional to g^2. The following empirical expressions can be used:

$$D_s(r;\omega) \cong \begin{cases} (\pi a^2/r^2)E_\infty \exp[-E_\infty \pi (g/\pi)^2], & g < \pi, \\ (\pi a^2/r^2)g^{-2}, & g > \pi. \end{cases} \quad (40)$$

The limiting value of $D_s(r;\omega)$ for $g \ll \pi$ is $(\pi a^2/r^2)E_\infty$, where

$$E_\infty = \lim_{ka\to\infty} \lim_{Y\to 0} \int_{Z=0}^{Z=ka} 8\left\{[u_1(Y,Z)Z/Y]^2 + [u_2(Y,Z)Z/Y]^2\right\}^2 Z^{-3}\left[1-\left(\frac{Z}{ka}\right)^2\right]^{-\frac{1}{2}} dZ, \quad (41)$$

$$= \int_{Z=0}^{Z=\infty} 8[J_1(Y,Z)]^4 Z^{-3} dZ = 0.46.$$

Since $r/r_0 = (g/\pi)^{-1}$ is the distance from the transducer to the scatterer location, normalized by the Rayleigh distance of the transducer $r_0 \equiv ka^2/2\pi$, it might be conceptually more evident to express the above relationship as

$$D_s(r;\omega) \cong \begin{cases} 4\pi/(ka)^2, & r/r_0 < 1, \\ \left[4\pi/(ka)^2\right](\pi^2 E_\infty)(r/r_0)^{-2} \\ \quad \times \exp\left[-E_\infty \pi (r/r_0)^{-2}\right], & r/r_0 > 1. \end{cases} \quad (42)$$

Numerical investigation of (39) indicates that (42) provides the value of $D_s(r;\omega)$ correct to within 1/2 dB for any value of r/r_0. Several conclusions can be made from Fig. 2 and (42): (1) when the distance from the transducer to the scattering volume is small compared to the Rayleigh distance, the diffraction correction varies slowly with distance, but it is inversely proportional to the frequency squared; (2) when the distance is much larger than the Rayleigh distance, the diffraction correction varies slowly with frequency, but it is inversely proportional to the distance squared; (3) beyond the Rayleigh distance, the diffraction correction function decreases slower than r^{-2}; (4) for a particular transducer, the diffraction reaches maximum at $r_{\max}/r_0 \approx 1.16$, where $D_s(r_{\max};\omega) \approx 1.13 \cdot 4\pi/(ka)^2 = 14.2/(ka)^2$.

The physical meaning of (42) becomes obvious when the case of an ensemble of discrete scatterers is reconsidered. Substituting (42) into (21) we find

$$\left\langle |\overline{P}_s(\mathbf{r} \in V;\omega)|^2 \right\rangle = |P_0(\omega)|^2 \cdot \eta(\omega) \cdot \frac{\pi a^2 l}{\bar{r}^2} E_\infty, \quad \text{for } \bar{r} \gg r_0. \quad (43)$$

Let us define $N_{\text{eff}} = n_0 \cdot \pi a^2 \cdot l \cdot E_\infty$ as the effective number of scatterers in the integration volume. It is the number of scatterers in the volume projected by the transducer surface along the length of sample, modified by the correction coefficient E_∞. Using this definition, we have

$$\left\langle |\overline{P}_s(\mathbf{r} \in V;\omega)|^2 \right\rangle = |P_0(\omega)|^2 \cdot \frac{N_{\text{eff}}\sigma_d}{\bar{r}^2}. \quad (44)$$

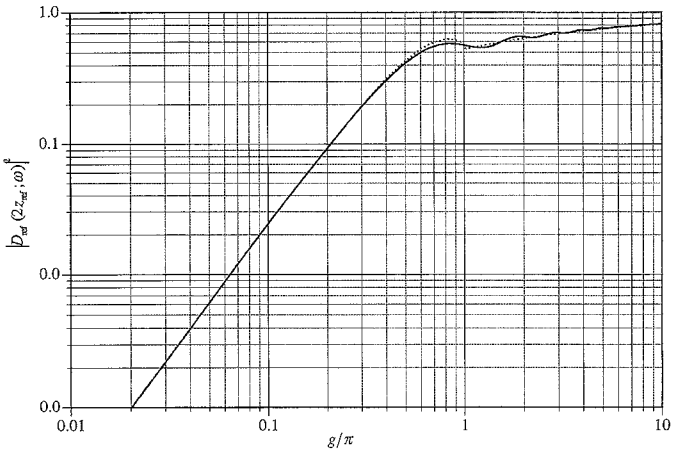

Fig. 3. Acoustic coupling correction $|D_{\text{ref}}(2z_{\text{ref}};\omega)|^2$ vs. g/π. For the flat transducer, $g = ka^2/2z_{\text{ref}}$, and z_{ref} is the distance from the transducer to the reference plate; For the focused transducer, the reference plate is positioned in the focal plane such that $z_{\text{ref}} = r_0$ and $g = G_p$. Dashed lines represent the approximations.

It states that the expected backscatter power from the scattering volume is equivalent to the backscatter power as measured at a distance $\bar{r}$ away from a single scatterer in a plane wave field with an effective cross-section of $\sigma_{\text{eff}} = N_{\text{eff}}\sigma_d$. The effective beam cross-section for the backscatter measurement is about 46% of the geometrical cross-section of the transducer in this case.

It is easy to demonstrate numerically that if $l \ll \bar{r}$, the mean diffraction correction function for the backscatter measurement can be replaced by the diffraction correction function at the mean distance from the transducer, *i.e.*, $\overline{D}_s(\mathbf{r} \in V;\omega) \cong D_s(\bar{r};\omega)$ From (42), it can be approximated by

$$\overline{D}_s(\mathbf{r} \in V;\omega) \cong \begin{cases} 4\pi/(ka)^2, & \bar{r}/r_0 < 1, \\ \left[4\pi/(ka)^2\right](\pi^2 E_\infty)(\bar{r}/r_0)^{-2} \\ \quad \times \exp\left[-E_\infty \pi (\bar{r}/r_0)^{-2}\right], & \bar{r}/r_0 > 1. \end{cases} \quad (45)$$

For a flat disk transducer with an element radius of a, the acoustic coupling function $D_{\text{ref}}(2z_{\text{ref}};\omega)$ is the Lommel diffraction function. A closed form of this function has been given by Rogers and Van Buren [9] and Chen *et al.* [7] as

$$D_{\text{ref}}(2z_{\text{ref}};\omega) = 1 - \exp(-ig)[J_0(g) + iJ_1(g)] \quad (46)$$

where z_{ref} is the distance from the transducer to the reference plate, and $g = ka^2/2z_{\text{ref}}$ can be considered as a normalized distance. The numerical value of $|D_{\text{ref}}(2z_{\text{ref}};\omega)|^2$ is shown in Fig. 3 as a function of g. The dependence of $|D_{\text{ref}}(2z_{\text{ref}};\omega)|^2$ on g can also be divided into two intervals, $g < \pi$ and $g > \pi$. For $g < \pi$, $|D_{\text{ref}}(2z_{\text{ref}};\omega)|^2$ is nearly proportional to g^2, while for $g > \pi$, the variation of $|D_{\text{ref}}(2z_{\text{ref}};\omega)|^2$ is relatively slow. The following empirical

expressions can be used

$$l|D_{\text{ref}}(2z_{\text{ref}};\omega)|^2 \cong \begin{cases} (g/2)^2 \exp\left[-E_\infty \pi (g/\pi)^2\right], & g < \pi, \\ \exp\left[-(2/\pi)(g/\pi)^{-1/2}\right], & g > \pi, \end{cases} \tag{47}$$

which can also be written as

$$l|D_{\text{ref}}(2z_{\text{ref}};\omega)|^2 \cong \begin{cases} \exp\left[-(2/\pi)(z_{\text{ref}}/r_0)^{1/2}\right], & z_{\text{ref}}/r_0 < 1, \\ (\pi/2)^2 (z_{\text{ref}}/r_0)^{-2} \\ \times \exp\left[-E_\infty \pi (z_{\text{ref}}/r_0)^{-2}\right], & z_{\text{ref}}/r_0 > 1. \end{cases} \tag{48}$$

The above discussion indicates that the sample volume and the reference plate can be positioned at different locations. If we allow $z_{\text{ref}} = \bar{r}$, (31) becomes

$$\eta(\omega) \cong \begin{cases} \dfrac{\langle |V_s(\mathbf{r} \in V;\omega)|^2 \rangle}{|V_{\text{ref}}(\bar{r};\omega)|^2} \cdot \dfrac{(ka)^2}{l \cdot 4\pi \cdot \exp\left[(2/\pi)(\bar{r}/r_0)^{1/2}\right]}, & \bar{r}/r_0 < 1, \\ \dfrac{\langle |V_s(\mathbf{r} \in V;\omega)|^2 \rangle}{|V_{\text{ref}}(\bar{r};\omega)|^2} \cdot \dfrac{(ka)^2}{l \cdot 4\pi \cdot 4E_\infty}, & \bar{r}/r_0 > 1. \end{cases} \tag{49}$$

Notice that the final correction is nearly proportional to the frequency squared.

B. The Focused Transducer

For a spherically focused transducer, the relative sensitivity of the transducer surface can be written as

$$U_T(\mathbf{r}_T;\omega)/U(\omega) = \begin{cases} \exp(-ik|\mathbf{r}_T|^2/2r_0), & |\mathbf{r}_T| \le a, \\ 0, & \text{Otherwise}, \end{cases} \tag{50}$$

where a is the radius of the active element, r_0 is the radius of curvature (geometric focal length). The radiation pattern of the focused transducer is more complicated than that of the flat disk transducer. However, most measurements with focused transducers are made near the focal area. The radiation pattern here has been given in different forms by several authors. Using the spherical coordinates shown in Fig. 1 and the diffraction pattern given in Chen *et al.* [8] , we have

$$|D(\mathbf{r};\omega)|^4 = (ka^2/r)^4 Y^{-4} \left[u_1(Y,Z)^2 + u_2(Y,Z)^2\right]^2 \tag{51}$$

where $Y = (ka^2/r)(1 - r\cos\theta/r_0)$, and $Z = ka\sin\theta$, and $u_1(Y,Z)$ and $u_2(Y,Z)$ are the Lommel functions of the first and second kind defined earlier. Letting $G_p = ka^2/2r_0$ stand for the pressure gain factor, and $g = G_p(r_0/r - 1)$,

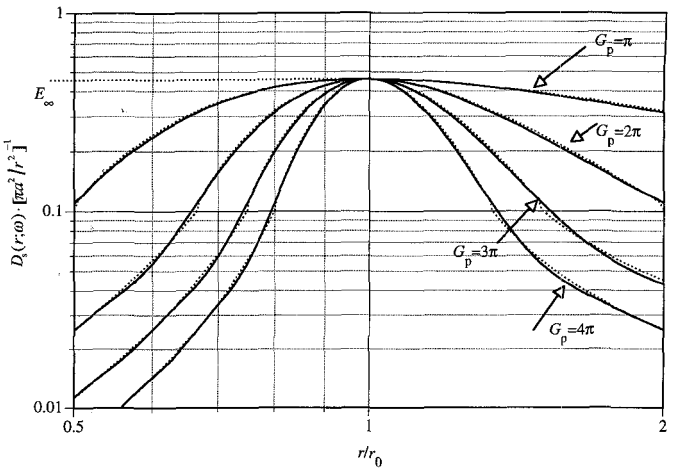

Fig. 4. Diffraction correction coefficient $D_s(r;\omega)$ vs. r/r_0, normalized by $\pi a^2/r^2$ for the focused transducer, for focusing factors $G_p = \pi$, 2π, 3π, and 4π. For $r_0 = 50.4$ mm and $a = 6.35$ mm, these correspond to 1.87 MHz, 3.75 MHz, 5.62 MHz, and 7.50 MHz, respectively. Dashed lines represent the approximations.

we have $Y = 2g + 2G_p(1 - \cos\theta)$. Substituting into (35), we again have

$$D_s(\mathbf{r};\omega) = \frac{\pi a^2}{r^2} \int_{Z=0}^{Z=ka} 8\left\{[u_1(Y,Z)Z/Y]^2 + [u_2(Y,Z)Z/Y]^2\right\}^2 Z^{-3} \left[1 - \left(\frac{Z}{ka}\right)^2\right]^{-\frac{1}{2}} dZ. \tag{52}$$

This expression is identical in form to (39) for the flat disk transducer. For high frequency ($ka \gg 1$) weakly focused transducers ($a/r_0 \ll 1$), the dependence of the diffraction correction on $|g|$ is very similar to that for the flat disk transducer, as shown in Fig. 2. This is not surprising, however, since the only difference between (39) and (52) is the definition of Y. It is easy to demonstrate numerically that $Y \approx 2g + Z^2/(kr_0) \approx 2g$ for values of Z which contribute significantly to the integral. Notice that the parameter g has values close to zero when the scatterer is near the focal area of the transducer, corresponding to the farfield of a flat transducer. The approximate form given in (44) translates to

$$lD_s(r;\omega) \cong \begin{cases} (\pi a^2/r^2) E_\infty \exp\left[-(E_\infty/\pi) G_p^2 (r_0/r - 1)^2\right], \\ (1 + \pi/G_p)^{-1} \le r/r_0 \le (1 - \pi/G_p)^{-1}, \\ (\pi a^2/r^2)\left[G_p(r_0/r - 1)^2\right]^{-2}, \\ \text{otherwise}. \end{cases} \tag{53}$$

Shown in Fig. 4 are the numerical values of $D_s(r;\omega)$ normalized by $\pi a^2/r^2$ as a function of r/r_0 for $G_p = \pi$, 2π, 3π, and 4π, calculated from (52) and (53). For weakly focused transducers with moderate pressure gain factors, the approximate expression given by (53) provides the correct value of $D_s(r;\omega)$ to within 1/2 dB. Several conclusions can

be made from Fig. 4 and (53): (1) when the scattering volume is close to the geometric focus, the diffraction correction varies slowly with frequency, and is inversely proportional to the distance squared; (2) at the geometric focus, $D_s(r;\omega) = (\pi a^2/r_0^2)E_\infty$ does not depend on frequency; (3) Beyond the focal point, the diffraction correction decreases faster than r^{-2}; (4) for a transducer with a particular geometry at a particular frequency, the diffraction correction reaches a maximum at $r_{\max} \approx r_0(1-2\pi^2/3G_p^2)$, where $D_s(r_{\max};\omega) \approx (\pi a^2/r_0^2)E_\infty \exp\left[(2/3)(G_p/\pi)^{-2}\right]$.

Similar to the flat disk transducer, it is easy to demonstrate numerically that, if $l \ll \bar{r}$, the mean diffraction correction function for the backscatter measurement can be replaced by the diffraction correction function at the mean distance from the transducer, *i.e.*, $\overline{D}_s(\mathbf{r} \in V;\omega) \cong D_s(\bar{r};\omega)$. From (53), it can be approximated by

$$\overline{D}_s(\mathbf{r} \in V;\omega) \cong \begin{cases} (\pi a^2/\bar{r}^2)E_\infty \exp\left[-(E_\infty/\pi)G_p^2(r_0/\bar{r}-1)^2\right], \\ (1+\pi/G-p)^{-1} \le \bar{r}/r_0 \le (1-\pi/G_p)^{-1}, \\ (\pi a^2/\bar{r}^2)\left[G_p(r_0/\bar{r}-1)^2\right]^{-2}, \\ \text{otherwise.} \end{cases} \tag{54}$$

The acoustic coupling function $D_{\text{ref}}(2z_{\text{ref}};\omega)$ for a spherically focused transducer has been given by Chen *et al.* as [7] (after the substitution $i = -j$ is made)

$$D_{\text{ref}}(2z_{\text{ref}};\omega) = -\frac{1}{x}\left\{\exp\left[\frac{-ig}{4}\left(x-\frac{1}{x}\right)\right]\operatorname{sinc}\left[\frac{g}{4}\left(x-\frac{1}{x}\right)\right] - \exp(-igx)[S_0(x,g)+iS_1(x,g)]\right\} \tag{55}$$

where $g = ka^2/2z_{\text{ref}}$, $x = 2z_{\text{ref}}/r_0 - 1$, and

$$\begin{cases} S_0(x,g) = \dfrac{2}{g}\displaystyle\sum_{n=0}^{\infty}\left[(-1)^n\left(\sum_{p=-2n,2}^{2n} x^p\right)J_{2n+1}(g)\right], \\ S_1(x,g) = \dfrac{2}{g}\displaystyle\sum_{n=0}^{\infty}\left[(-1)^n\left(\sum_{p=-(2n+1),2}^{2n+1} x^p\right)J_{2n+2}(g)\right] \end{cases} \tag{56}$$

Generally, evaluation of (57–58) is necessary to obtain $|D_{\text{ref}}(2z_{\text{ref}};\omega)|^2$. When the reference plate is positioned in the focal plane, *i.e.* $z_{\text{ref}} = r_0$, we have $x = 1$ and $g = G_p$. Then the functions $S_0(x,g)$ and $S_1(x,g)$ reduce to $J_0(G_p)$ and $J_1(G_p)$, respectively, and (55) becomes [7]

$$D_{\text{ref}}(2r_0;\omega) = -1\left\{1-\exp(-iG_p)\left[J_0(G_p)+iJ_1(G_p)\right]\right\}. \tag{57}$$

The numerical value of $|D_{\text{ref}}(z_{\text{ref}};\omega)|^2$ as a function of G_p is identical to that for the flat disk transducer in this case. Again the coupling function $|D_{\text{ref}}(z_{\text{ref}};\omega)|^2$ is only weakly dependent on the acoustic frequency when $G_p > \pi$, and this function can be replaced by the simple form given in (34). Because G_p is the pressure gain factor of the focused transducer, the condition $G_p > \pi$ is satisfied for most cases of practical interest. Therefore, we have

$$|D_{\text{ref}}(2r_0;\omega)|^2 \cong \exp\left[-(2/\pi)(G_p/\pi)^{-1/2}\right], \quad G_p > \pi. \tag{58}$$

If we allow $z_{\text{ref}} = \bar{r} = r_0$, (31) becomes

$$\eta(\omega) \cong \frac{\langle|V_s(\mathbf{r}\in V;\omega)|^2\rangle}{|V_{\text{ref}}(r_0;\omega)|^2}\cdot\frac{r_0^2}{l\cdot\pi a^2\cdot E_\infty} \cdot \exp\left[-(2/\pi)(G_p/\pi)^{-1/2}\right]. \tag{59}$$

Notice that there is only a weak frequency dependence in the final correction.

IV. Discussions

We now demonstrate that the AIUM recommended Sigelmann-Reid [2] formulation can be derived as a special case of our formulation. The Sigelmann-Reid formulation can be written as ((23) in [2])

$$\eta_{S-R}(\omega) = \frac{\langle|V_s(\mathbf{r}\in V;\omega)|^2\rangle}{|V_{\text{ref}}(\bar{r};\omega)|}\frac{\bar{r}^2}{4S_{\text{eff}}l}, \tag{60}$$

where the attenuation correction has been suppressed, l is used in place of $c(t_2-t_1)/2$, and S_{eff} is the effective beam cross-sectional area. Using their recommendation, the -3 dB beam area is used as the effective beam cross-sectional area, *i.e.*

$$S_{-3\text{ dB}} = \pi(\bar{r}\sin\theta_{-3\text{ dB}})^2 = \pi\bar{r}^2\left(\frac{1.616}{ka}\right)^2. \tag{61}$$

When the same experimental condition is used, and calibration is performed by substituting the sample volume with a perfect reflector ($z_{\text{ref}} = \bar{r}$), (31) can also be written in the form of (60), except the effective beam cross-sectional area is

$$S_{\text{eff}} = \pi\bar{r}^2\frac{4E_\infty}{(ka)^2}, \tag{62}$$

(61) and (62) are identical except for a numerical constant. The difference in the numerical constant can be explained by the fact that the -3 dB beam cross-sectional area is derived from $|D(\mathbf{r};\omega)|^2$, while in our formulation the effective beam area is derived from $|D(\mathbf{r};\omega)|^4$ which has a narrower lateral distribution. We propose that the effective beam cross-section defined in (62) be used in the Sigelmann-Reid formulation, instead of the -3 dB beam cross-sectional area.

It is important to stress that the Sigelmann-Reid method is based on the assumption that the pressure distribution has reached spherical spreading at the location of the sample volume, *i.e.* the pressure amplitude decays as $1/r$. This requires that $\bar{r} \gg ka^2/2\pi$, the latter being the Rayleigh distance of the transducer. A safe estimate of the distance is $\bar{r} \ge ka^2/2$. However, the -3 dB beamwidth is

comparable with the diameter of the transducer at these locations, and poor spatial resolution is achieved. Also, the required distance becomes prohibitively large for relatively high frequencies such that the signal-to-noise ratio poses an additional difficulty to the accurate measurement of backscatter coefficient. For example, for $f = 5$ MHz and $a = 6.35$ mm, we have $\bar{r} \geq ka^2/2 = 0.40$ m. For these parameters, the sample should probably be placed at the Rayleigh distance of the transducer, and the exact numerical solution of (20) and (28) or the approximate solutions in (42) and (48) should be used for the final data reduction.

As for the spherically focused transducer, many formulations exist. The following formulation for the backscatter coefficient from pulse-echo measurement was presented by Madsen *et al.* [4]

$$\eta_{\text{M-I-Z}}(\omega) = \frac{\left\langle |V_s(\mathbf{r} \in V;\omega)|^2 \right\rangle}{(\tau/2\pi)^2 a(\omega)}, \tag{63}$$

where $\left\langle |V_s(\mathbf{r} \in V;\omega)|^2 \right\rangle$ is the averaged power spectrum of the gated radio-frequency signal from the scattering volume, $a(\omega)$ is defined as

$$a(\omega) = \iiint_V dV(\mathbf{r}) \left| \int_{-\infty}^{\infty} d\omega' T(\omega') B(\omega') \times \operatorname{sinc}\left[\frac{(\omega-\omega')\tau}{2\pi}\right] A_0^2(\mathbf{r};\omega) \right|^4, \tag{64}$$

τ is the receive gate duration, $T(\omega)B(\omega)$ represents the system response function, and $A_0(\omega)$ is defined as

$$A_0(\mathbf{r};\omega) = \iint_{S_T} \frac{\exp(ikr'_T)}{r'_T} dS(\mathbf{r}_T). \tag{65}$$

Notice that $A_0(\mathbf{r};\omega) = (i2\pi/k) \cdot D(\mathbf{r};\omega)$ where $D(\mathbf{r};\omega)$ is the radiation pattern defined in (3), except that a relative phase delay and amplitude shading of the transducer elements are allowed in our formulation. The sinc function in (64) is due to the finite gate duration. If we ignore the effect of the gate duration (see the discussion by Wear and Popp [10]), by setting $\operatorname{sinc}[(\omega-\omega')\tau/2\pi] \cong (2\pi/\tau)\delta(\omega-\omega')$, then (64) becomes

$$\begin{aligned} a(\omega) &\cong |T(\omega)B(\omega)|^2 (2\pi/\tau)^2 \iiint_V dV(\mathbf{r}) |A_0^2(\mathbf{r};\omega)|^2 \\ &= |T(\omega)B(\omega)|^2 (2\pi/\tau)^2 (2\pi S/k)^2 \cdot l \cdot \overline{D}_s(\mathbf{r} \in V;\omega) \end{aligned} \tag{66}$$

where $\overline{D}_s(\mathbf{r} \in V;\omega)$ is the mean diffraction correction for backscatter coefficient defined in (20). The system response function $T(\omega)B(\omega)$ is obtained from

$$T(\omega)B(\omega) = V_{\text{ref}}(\omega) \left[R \iint_{S_R} A_0(\mathbf{r};\omega) dS(\mathbf{r}_R) \right]^{-1}, \tag{67}$$

where $V_{\text{ref}}(\omega)$ is the Fourier transform of the radio frequency voltage signal from a reference reflector and R is the reflection coefficient of the reference reflector. Again, since $A_0(\mathbf{r};\omega) = (i2\pi/k) \cdot D(\mathbf{r};\omega)$, we have

$$|T(\omega)B(\omega)|^2 = |V_{\text{ref}}(\omega)|^2 (2\pi S/k)^2 |D_{\text{ref}}(2z_{\text{ref}};\omega)|^{-2}. \tag{68}$$

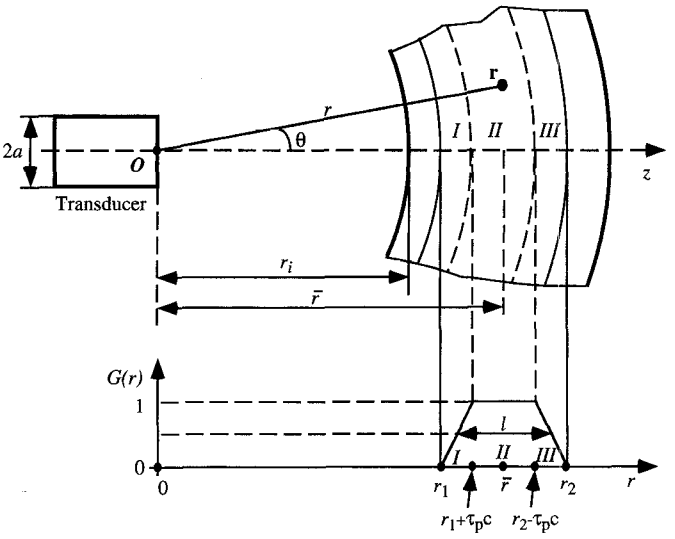

Fig. A1. A more realistic scattering geometry for tissue characterization, and the definition of the spatial receive gate.

Combining (63), (66) and (68), the backscatter coefficient is

$$\eta_{\text{M-I-Z}}(\omega) \cong \frac{\left\langle |V_s(\mathbf{r} \in V;\omega)|^2 \right\rangle}{|V_{\text{ref}}(2z_{\text{ref}};\omega)|^2} \cdot \frac{|D_{\text{ref}}(2z_{\text{ref}};\omega)|^2}{l \cdot \overline{D}_s(\mathbf{r} \in V;\omega)}, \tag{69}$$

which is identical to our formulation as given by (31).

V. Conclusion

A new formulation for measuring the backscatter coefficient is presented. System calibration is accomplished by using a reference plate (a perfect reflector), as has been suggested by others. Two nondimensional correction functions are defined as integrals of the diffraction pattern of the transducer. Approximate solutions are provided for two useful cases, the flat disk transducer and the spherically focused transducer. These solutions are easy to evaluate numerically. For the flat disk transducer, the final data reduction involves a correction proportional to the frequency squared, as predicted by Sigelmann and Reid [2]. Our formulation agrees with Sigelmann and Reid [2] when the same experimental condition is used, except for a numerical constant. It also suggests that the sample volume and the reference plate could be placed in the nearfield for a flat transducer. For the focused transducer, our formulation agrees with Madsen *et al.* [4] when the effect of the finite receive gate is ignored. The final data reduction is only weakly dependent on the frequency when the sample volume is close to the focal area.

Appendix A. The Spatial Receive Gate

A more practical experimental set-up is shown in Fig. A1. The transmitted pulse has a finite duration τ_p,

and the receive gate duration is $\tau = t_2 - t_1$. Due to the finite pulse duration the gated received signal includes scattering information from the three volumes marked *I*, *II* and *III* depicted in Fig. A1, assuming $\tau > \tau_p$. The scattering signals are received completely for scatterers in region *II*, and the scattering signals are received partially for scatterers in region *I* and *III*. This situation justifies the definition of a spatial receive gate $G(r)$ shown in Fig. A1, with

$$G(r) = \begin{cases} \dfrac{r - r_1}{\tau_p c}, & r_1 < r < r_1 + \tau_p c, \\ 1, & r_1 + \tau_p c < r < r_2 - \tau_p c, \\ \dfrac{r_2 - r}{\tau_p c}, & r_2 - \tau_p c < r < r_2, \\ 0, & \text{otherwise.} \end{cases} \tag{A1}$$

Here, $r_1 = c_0 t_i/c + c(t_1 - t_i)/2$, $r_2 = c_0 t_i/2 + c(t_1 - t_i)/2$, t_i is the arrival time of the medium-tissue interface, and $r_i = c_0 t_i/2$ is the distance from the transducer to the interface. The effective sample length, l, is therefore:

$$\begin{aligned} l &= \int_{r_1}^{r_2} G(r)dr = r_2 - r_1 - c\tau_p/2 \\ &= c(t_2 - t_1 - \tau_p)/2, \end{aligned} \tag{A2}$$

and the mean distance from the transducer to the sample, $\bar{r}$, is

$$\bar{r} = \int_{r_1}^{r_2} rG(r)dr = (r_2 + r_1)/2. \tag{A3}$$

The mean diffraction correction in (31) can be replaced by

$$\overline{D}_s(\mathbf{r} \in V; \omega) = \frac{1}{l} \int_{r_1}^{r_2} G(r) D_s(r; \omega) dr, \tag{A4}$$

which reduces to (31) if $\tau_p \ll \tau$.

Appendix B. The Attenuation Correction

When attenuation is considered, the diffraction pattern of the transducer $D(\mathbf{r})$ is replaced by $D(\mathbf{r}) \exp[-\alpha_0 r_i - \alpha(r - r_i)]$, correct to the lowest order of approximation. Here, α_0 is the attenuation coefficient of the medium, and α is the attenuation coefficient of the tissue. The effect of attenuation can be obtained by inspection of (A4):

$$\begin{aligned} \overline{D}_s(\mathbf{r} \in V; \omega) = \frac{1}{l} \int_{r_1}^{r_2} & G(r) D_s(r; \omega) \\ & \times \exp[-4\alpha_0 r_i - 4\alpha(r - r_i)] dr. \end{aligned} \tag{B1}$$

Keeping the definition of diffraction correction coefficient, and allowing $l \ll \bar{r}$, we have the following approximation for the attenuation correction coefficient

$$\begin{aligned} A_s(\mathbf{r} \in V; \omega) \cong \frac{1}{l} \int_{r_1}^{r_2} & G(r) \\ & \times \exp[-4\alpha_0 r_i - 4\alpha(r - r_i)] dr. \end{aligned} \tag{B2}$$

When the gate function in (A1) is used, we find

$$\begin{aligned} A_s(\mathbf{r} \in V; \omega) \cong & \exp[-4\alpha_0 r_i - 4\alpha(r - r_i)] \\ & \cdot \frac{\exp[2\alpha\tau_p c] - \exp[-2\alpha\tau_p c]}{4\alpha\tau_p c} \cdot \frac{\exp[2\alpha l] - \exp[-2\alpha l]}{4\alpha l}. \end{aligned} \tag{B3}$$

When attenuation is considered, the coupling function $|D_{\text{ref}}(2z_{\text{ref}}, \omega)|^2$ is replaced by $|D_{\text{ref}}(2z_{\text{ref}}; \omega)|^2 \cdot \exp(-4\alpha_0 z_{\text{ref}})$, as is apparent from (28). So the total attenuation correction is

$$\begin{aligned} A_s(\mathbf{r} \in V; \omega) \cong & \exp[-4\alpha_0(r_i - z_{\text{ref}}) - 4\alpha(r - r_i)] \\ & \cdot \frac{\exp[2\alpha\tau_p c] - \exp[-2\alpha\tau_p c]}{4\alpha\tau_p c} \cdot \frac{\exp[2\alpha l] - \exp[-2\alpha l]}{4\alpha l}. \end{aligned} \tag{B4}$$

This correction is identical to that given by Sigelmann and Reid [2] if α_0 is allowed to vanish in the above expression.

When $\alpha l \ll 1$ (due to either low attenuation efficient or small sample length), the last two terms of (B4) approaches unity. We have therefore

$$A_s(\mathbf{r} \in V; \omega) \cong \exp[-4\alpha_0(r_i - z_{\text{ref}}) - 4\alpha(\bar{r} - r_i)] \tag{B5}$$

References

[1] AIUM, *Standard Methods for Measuring Performance of Pulse-Echo Ultrasound Imaging Equipment*, 1990.

[2] R. A. Sigelmann and J. M. Reid, "Analysis and measurement of ultrasonic backscattering from an ensemble of scatterers excited by sine-wave bursts," *J. Acoust. Soc. Amer.*, vol. 53, pp. 1351–1355, 1973.

[3] J. A. Campbell and R. C. Waag, "Normalization of ultrasonic scattering measurements to obtain average differential scattering cross sections for tissues," *J. Acoust. Soc. Amer.*, vol. 74, pp. 393–399, 1983.

[4] E. L. Madsen, M. F. Insana, and J. A. Zagzebski, "Method of data reduction for accurate determination of acoustic backscatter coefficients," *J. Acoust. Soc. Amer.*, vol. 76, pp. 913–923, 1984.

[5] G. Yao, V. L. Newhouse, and J. Satrapa, "Estimation of scatterer concentration from randomly scattered signals," *J. Acoust. Soc. Amer.*, vol. 84, pp. 771–779, 1988.

[6] P. M. Morse and K. U. Ingard, *Theoretical Acoustics*, Princeton, NJ: Princeton University Press, 1986, Chapter 8.

[7] X. Chen, K. Q. Schwarz, and K. J. Parker, "Acoustic coupling from a focused transducer to a flat plate and back to the transducer," *J. Acoust. Soc. Amer.*, vol. 95, pp. 3049–3054, 1994.

[8] X. Chen, K. Q. Schwarz, and K. J. Parker, "Radiation pattern of a focused transducer: a numerically convergent solution," *J. Acoust. Soc. Amer.*, vol. 94, pp. 2979–2991, 1993.

[9] P. H. Rogers and A. L. Van Buren, "An exact expression for the Lommel diffraction correction integral," *J. Acoust. Soc. Amer.*, vol. 55, pp. 724–728, 1974.

[10] K. A. Wear and R. L. Popp, "Theoretical Analysis of a Technique for the Characterization of Myocardium Contraction Based Upon Temporal Correlation of Ultrasonic Echoes," *IEEE Trans. Ultrason., Ferroelect., Freq. Contr.*, vol. UFFC-34, pp. 368–375, 1987.

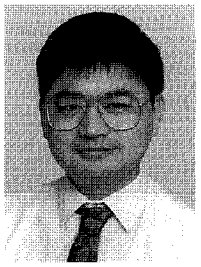

Xucai Chen was born in Jiangsu Province, China on March 5, 1962. He finished his undergraduate training at the China Mining Institute in 1982. He received his M.S., M.Phil. and Ph.D. from Yale University in 1986, 1989, and 1991 respectively, in the Program in Engineering and Applied Science. He completed his post-doctoral training in the Departments of Medicine (Cardiology) and Department of Electrical Engineering at the University of Rochester, Rochester NY in 1993. He is currently an assistant professor of Medicine and a scientist in Electrical Engineering at the University of Rochester. He has been involved in the research of therapeutic and diagnostic ultrasound. He is particularly interested in acoustic scattering, acoustic radiation force, and new ultrasound imaging modality for blood flow visualization using ultrasound contrast agent.

Daniel Phillips was born in Rochester, NY in 1956. He received the BS degree in Electrical Engineering from SUNY/Buffalo in 1979. From 1978 until 1992, he was employed as a systems engineer involved with automated test in the industrial sector as well as medical data acquisition and analysis in both clinical and laboratory environments. He was accepted in the graduate program in Electrical Engineering at the University of Rochester in 1992, receiving the MSEE in 1994 and is currently working toward a PhD with a concentration in biomedical ultrasound. His current research involves simulation and analysis of ultrasonic scattering in tissue.

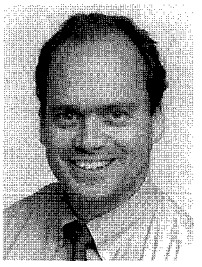

Karl Q. Schwarz was born on June 29, 1957. He received an A.B. degree in Physics from Bowdoin College, Brunswick, Maine in 1979, and an M.D. degree from the University of Rochester, Rochester, NY in 1983. Dr. Schwarz completed his internal medicine residency at Strong Memorial Hospital in Rochester, NY in 1986 and his cardiology fellowship at the University of Rochester in 1989. Since that time he has been a staff cardiologist at the University of Rochester and has been director of the Echocardiography Laboratory since 1992. He is currently an associate professor of medicine and a member of the Center for Biomedical Ultrasound in Rochester, NY. His primary research interest is in the behavior of small gas bubbles in a sound field. For the past five years he has worked primarily with the echo contrast agent from Schering AG (Berlin, Germany) and its effect on Doppler ultrasound signals. Recently, his research work has included harmonic imaging techniques and echo contrast. As director of the Echocardiography Laboratory, Dr. Schwarz is involved in many clinical research projects as well. In addition, Dr. Schwarz is an avid programmer and recently completed work on a clinical data management system which is currently for sale by Acuson, Inc. (Mountain View, CA) under the name CasePro. Dr. Schwarz is a fellow of the American College of Cardiology and the American Heart Association. He is also a member of the American Society of Echocardiography.

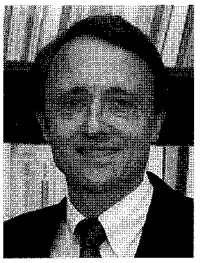

Kevin J. Parker (S'79–M'81–SM'87–F'95) received the BS degree in engineering science, summa cum laude, from SUNY at Buffalo in 1976. Graduate work in electrical engineering was done at MIT, with MS and PhD degrees received in 1978 and 1981. From 1981 to 1985 he was an assistant professor of electrical engineering and radiology. Dr. Parker has received awards from the National Institute of General Medical Sciences (1979), the Lilly Teaching Endowment (1982), the IBM Supercomputing Competition (1989), the World Federation of Ultrasound in Medicine and Biology (1991). He is a member of the IEEE Sonics and Ultrasonics Symposium Technical Committee and serves as reviewer and consultant for a number of journals and institutions. He is also a member of the IEEE, the Acoustical Society of America, and the American Institute of Ultrasound in Medicine. He has been named a fellow in both the IEEE and the AIUM for his work in medical imaging. Dr. Parker's research interests are in medical imaging, linear and nonlinear acoustics, and digital halftoning.